Authors: Anna Granfors (Institutionen för kemi och molekylärbiologi); Maria Andersson (Institutionen för kemi och molekylärbiologi); Melissa Chierici (Institutionen för kemi och molekylärbiologi); Agneta Fransson (Institutionen för geovetenskaper); Katarina Gårdfeldt (Institutionen för kemi- och bioteknik, Chalmers); Anders Torstensson (Institutionen för biologi och miljövetenskap); Angela Wulff (Institutionen för biologi och miljövetenskap); Katarina Abrahamsson (Institutionen för kemi och molekylärbiologi)

Title: Biogenic halocarbons in young Arctic sea ice and frost flowers

Marine Chemistry Volume 155, 20 September 2013, Pages 124–134
http://dx.doi.org/10.1016/j.marchem.2013.06.002

Biogenic Halocarbons in Young Arctic Sea Ice and Frost Flowers

Anna Granfors[a], Maria Andersson[a1], Melissa Chierici[a], Agneta Fransson[b2], Katarina Gårdfeldt[c], Anders Torstensson[d], Angela Wulff[d] and Katarina Abrahamsson[a]*

a. Department of Chemistry and Molecular Biology, University of Gothenburg, SE-412 96, Göteborg, Sweden

b. Department of Earth Sciences, University of Gothenburg, SE-405 30, Göteborg, Sweden.

c. Centre for Environment and Sustainability - Chalmers University of Technology/University of Gothenburg, SE-412 96, Göteborg, Sweden

d. Department of Biological and Environmental Sciences, University of Gothenburg, P.O. Box 461, SE-405 30 Göteborg, Sweden

Between first and last author, authors appear in alphabetical order

*Corresponding author.

e-mail address: k@chem.gu.se (K. Abrahamsson).

[1] Present adress ESSIQ AB, SE- 421 50 Västra Frölunda, Sweden
[2] Present adress Norwegian Polar Institute, Fram centre, Tromsø, Norway

Abstract

The fate of halocarbons, naturally produced volatile halogenated organic compounds, in young Arctic sea ice was studied to better understand the role of sea ice in halocarbon cycling. In early spring, halocarbons were measured in sea ice frozen in core holes, during 12 days of formation and freezing. In order to understand which factors govern halocarbon concentration and distribution, salinity, temperature and biological parameters were monitored in the growing sea ice. It was found that sea ice participates in the cycling of halocarbons between sea and air. Sea ice concentrations and distributions of these compounds were influenced by production in the ice, where ice-inhabiting microorganisms caused local increases in halocarbon concentrations. Moreover, the halocarbon ice concentration decrease/change with time did not follow ice salinity, suggesting that additional removal processes caused sea ice to be a source of halogens to overlying air. The net production rate of bromoform in the surface of newly frozen ice was estimated to 14 pmol L^{-1} d^{-1} and the maximum removal rate was 18 pmol L^{-1} d^{-1}. In addition frost flowers on newly formed sea ice were identified as contributors of halocarbons to the atmosphere with halocarbon concentrations in the same order of magnitude as in sea ice brine.

Keywords: biogenic halocarbons; bromoform; degassing; young sea ice; frost flowers; ice algae; heterotrophic bacteria

1. Introduction

Halocarbons, naturally occurring volatile halogenated organic compounds, are a source of halogens to the atmosphere, and can be photolyzed to form reactive halogen species (Simpson et al., 2007). Reactive halogens are known to contribute significantly to the destruction of ozone in the polar stratosphere and the underlying troposphere. Halocarbons are biologically produced in marine environments by macro- and microalgae (Collén et al., 1994; Ekdahl et al., 1998, Carpenter and Liss, 2000). In ice-covered oceans, sea ice can act as a source of halocarbons when they are produced by microorganisms within sea ice brine (Sturges et al., 1992; Karlsson, 2012).

Although research has been undertaken into halocarbon production and distribution in marine environments, there are few studies of halocarbons in Arctic sea ice (Sturges et al., 1997). In addition, the processes that govern halocarbon concentration and distribution in sea ice during freezing are poorly understood. An understanding of these is necessary in order to estimate sources of halocarbons to the atmosphere in this region. Sea ice has recently gained attention for its role in the interactions between ocean, sea ice, snow and atmosphere (Abbatt, 2012). Of special interest is the connection between ozone depletion and newly formed sea ice, where brine slush or frost flowers are possible sources of halogens (Jones et al., 2006; Simpson et al., 2007).

For some halocarbons, the activity of ice-living microorganisms, such as algae and heterotrophic bacteria, may affect their concentrations in sea ice. The interpretation of measurements of biogenic halocarbons in sea ice is complicated by variations originating from the influence of biological activity, and the fact that most samples from the field are spot samples from different locations. An attempt to overcome this problem was made in this study, which consists of a time series of samples from one experimental site in Ny-Ålesund,

Svalbard, where the variability of halocarbons, and the biological parameters: microalgal and bacterial abundance, photosynthetic yield and bacterial carbon production were studied simultaneously during freezing of sea ice.

The aim of the study was to investigate the fate of halocarbons in Arctic sea ice, focusing on the potential flux to the atmosphere during freezing in a natural environment. Concentration and depth distribution of the measured parameters were studied in ice cores from old ice and from newly frozen ice (1 to 12 days old). Biological and physical processes affecting halocarbon concentrations and ice-air flux are discussed.

2. Materials & Methods

2.1 Study site

The freezing experiment was carried out in Ny-Ålesund, Svalbard from 21 March to 2 April 2010. The experimental site was a small bay (Thiisbukta, Lat 78° 56´ N, Long 11° 56´ E), located 500 m from Ny-Ålesund village, and the ice was about two months old at the beginning of the experiment (personal communication with Bendik Halgunset, research advisor, Kings Bay AS). The total surface area of the bay was approximately 10000 m^2, and approximately 1 % was used as experimental site. At the beginning of the experiment the ice thickness was measured to be 27 cm. Thiisbukta was influenced by strong tides, which meant that the ice occasionally came in contact with the sediment. A few times during the experiment, sediment was found both in newly frozen and control ice cores. In the samples containing sediment, very high halocarbon concentrations were often detected and these samples were excluded from the displayed results.

2.2 Meteorological parameters

Air temperature and wind speed during the experiment were obtained from the Norwegian Meteorological Institute at their website; www.met.no (measuring site is 570 m from the study area), and photosynthetically active radiation (PAR) was obtained from our own radiation measurements (Figure 1a-c). The average daily air temperatures were between -10 °C and -15 °C, warmest on experimental day 10 and coldest on experimental day 6. Variation of average wind speed per day was between 1 and 7 m s^{-1} with a maximum value on experimental day 9. The highest solar radiation was measured on experimental day 5 Radiation measurements in the ice showed that 8 % of incident PAR remained at 35 cm depth (mid-day).

2.3 Sampling and experimental design

On experimental day 0, 50 holes were drilled through the ice using a gasoline powered ice-corer, with a diameter of 0.12 m. The holes were evenly distributed in an area of about 100 m^2. Care was taken so that no ice debris from the coring was left in the holes. The water in the holes was then left to re-freeze during the experiment, and re-frozen cores were sampled as single samples nearly every day (in total 10 occasions) during the 12-day experiment. Newly frozen ice-cores were randomly sampled from different boreholes for halocarbon measurements on experimental days 1, 2, 3, 5, 6, 8, 9, 10, 11 and 12. No hole was sampled more than once.

The old ice covering the bay was used as a reference (control) for halocarbon measurements, and was sampled on the same days as the newly frozen ice. This experiment treats the control ice as homogeneous with respect to location at the sampling site, since the cores drilled on day 0 all had the same thickness and structure (visually inspected), which implied that the area was covered with relatively homogenous ice. Moreover, a duplicate sample was analyzed from the control ice on day 0 and the variation between the inventory

concentrations (mean bulk concentration) of the two cores was 17 % (of average mean bulk concentration) for CH_2ClI, 2.7 % for CH_2BrI and 7.4 % for $CHBr_3$, which was found to be an acceptable variation for our study.

The newly frozen ice cores, sampled from the various holes, were assumed to have the same concentration and depth distribution of halocarbons independent of their spatial distribution at the experimental site. This assumption was found to be reasonable for the experiment, since duplicate ice cores sampled at two occasions were similar in concentration and depth distribution. Variations (in percent of mean concentration) between duplicates at the same depth were on average 26 % for CH_2ClI, 27 % for CH_2BrI and 17 % for $CHBr_3$. The duplicate samples of newly frozen ice cores were taken from the same sampling site, and were independent samples which were not included in the time series.

Ice cores for halocarbon analysis were divided into 5-cm sections and individually packed in gas-tight Tedlar© bags. After emptying the bags of surrounding air, the ice samples were thawed in darkness at room temperature for approximately 24 h. Sea ice temperature was measured immediately after the ice core was recovered at 5 cm intervals using a digital thermistor (Amadigit) with an accuracy of 0.1ºC. Separate ice cores were sampled for microbiological abundance and activity within 20 cm radius from the cores sampled for halocarbon analysis. These were immediately wrapped in black plastic to protect the algae from light stress.

Sea ice brine was collected at the study site in shallow (10 to 15 cm deep) “sack holes”. This means that the ice was partially cored to leave a core-hole in its surface. This was done to 10-15 cm depth in the ice to ensure that the seawater from below did not enter the hole. Brine that drained from the surrounding ice into the hole was sampled with a syringe. This method allowed sampling of large brine volumes but had the disadvantage that the ice volume

feeding the collected sample was unknown. The sack holes were covered with a plastic lid, during brine seeping, to minimize gas exchange with the atmosphere. During our study the seeping time for brine was about 1 hour to allow for sufficient sample volume, hence, some gas exchange may have taken place. Under-ice water (UIW) was collected with a glass bottle on a shaft (custom built) through the bore hole.

Frost flowers were sampled approximately 200 m from our study site on experimental days 6 and 7 with a Teflon ladle from a surface area of 1 m^2 for each sample. The samples were packed in Tedlar© bags. After emptying the bags of surrounding air, the frost flower samples were thawed in darkness at room temperature. The melted volume was approximately 1L. Salinity of the melted sea ice and frost flowers, brine and UIW were measured using a conductivity meter (WTW Cond 330i, Germany) with a precision and accuracy of ±0.05.

2.4 Halocarbon analyses

Halocarbons were determined in the samples according to the method described in Mattsson et al. (2012). Two identical analytical systems were used and consisted of custom built purge and trap systems coupled to gas chromatographs with electron-capture detectors (Varian 3800). The traps were Vocarb® 3000 used with a trap temperature of -5 ºC and a desorb temperature of 225 ºC. Separations of halocarbons were performed using an Agilent DB-624 wide bore column (60 m, I.D. 0.32 mm, film 1.80 µm). The systems were calibrated with external standards of CH_3I (Sigma-Aldrich, 99.5%), CH_3CH_2I (Merck, 99%), CH_3CHICH_2 (Fluka, >98%), CH_2Br_2 (Merck, 99%), $CH_3CH_2CH_2I$ (Aldrich, 99%), $CHBrCl_2$ (Fluka, >98%), CH_2ClI (Fluka, >97%), $CH_3CHICH_2CH_3$ (Fluka, >99%), $CHBr_2Cl$ (Fluka, >97%), $CH_2ICH_2CH_2CH_3$ (Fluka, >99%), CH_2BrCH_2Br (unknown), CH_2BrI (Fluka), $CHBr_3$ (Sigma-Aldrich, 97,9%) and CH_2I_2 (Sigma-Aldrich, 98%) diluted from a stock solution in methanol (Sigma-Aldrich, suitable for purge and trap analysis) in seawater to give final

concentrations of pmol L^{-1} in the purge chamber. The systems were calibrated with standards run every day for the entire campaign, in total 16 days. The detection limits for the compounds are in the fmol L^{-1} range, and the overall precision for the compounds were between 1 and 5%.

The measured bulk ice halocarbon concentrations were corrected for (*i.e.* divided by) brine volume, estimated from ice temperature and bulk salinity according to equation given by Frankenstein and Garner (1967): $v_b/v = S_i(0.0532\text{-}4.919/T_i)$, for ice temperatures ($T_i$) between -22.9°C and -0.5°C, and where v_b/v is the brine volume (per cent of total core volume), and S_i is the bulk ice salinity. The brine volume corrected values represent the halocarbon concentrations in brine, assuming that the halocarbons are completely dissolved in the liquid brine. The fact that bulk ice concentrations divided by brine volume were similar to concentrations measured directly in the sampled brine strongly indicated that this was a reasonable assumption.

2.5 Microbiological analyses

Microalgal and heterotrophic bacterial abundances and activities in control ice were measured on experimental days 0, 2, 5, 8 and 10 (single samples), and newly frozen was sampled experimental days 1, 2 3, 5, 6, 8 and 10 (single samples, triplicate day 10). All ice processing for microbiological analyses was performed at 0 °C. To separate the brine from the ice matrix, subsections were cut from each 5 cm section and the ice was centrifuged at 1 400 RPM at 0 °C for 4 minutes (Weissenberger er al., 1992). Maximum quantum yield of photosynthesis (F_v/F_m) was determined in the drained brine with a WATER-PAM chlorophyll fluorometer (Walz Mess- und Regeltechnik, Effeltrich, Germany) after ~10 min of dark acclimatization. Pulse Amplitude Modulated (PAM) fluorometry is a quick and non-invasive tool for estimating the momentary photosynthetic efficiency of photosystem II. Minimum

fluorescence (F_o) was determined by applying a low level of radiation intensity to the sample, and the maximum fluorescence (F_m) by exposing the sample to a short saturation pulse of measuring light (>1500 µmol photons m^{-2} s^{-1} for 0.6 s). Variable fluorescence ($F_v = F_m - F_o$) and maximum quantum yield (F_v/F_m) was determined for all samples.

Bacterial production (BP) in the drained brine was determined by (^{3}H)-leucine incorporation (Smith and Azam, 1992). Samples (1.3 ml) were incubated in darkness with final concentration of 35 nmol L^{-1} leucine (Perkin Elmer, Boston, MA, USA) for 1 h at *in situ* temperature. Prior to incubation, tricloracectic acid (TCA) was added to one sample (5 %, final concentration) to act as blank. The remaining samples were terminated with TCA (5 %, final concentration) after (^{3}H)-leucine incubation. Samples were centrifuged (13,400 rpm at 10° C for 10 minutes) and rinsed twice with 5 % TCA, and 1 ml scintillation cocktail (Ultima Gold) was added. The incorporated radioactivity in the samples was analysed in a liquid scintillation counter (Packard 1600CA Tri-Carb, Meriden, CT, USA). Leucine incorporation was converted to bacterial carbon production (BCP) assuming 2.0×10^{-14} g C $cell^{-1}$ (Lee and Fuhrman, 1987) and using the cell to carbon factor 7.0×10^{16} cells $mole^{-1}$ leucine incorporated (Riemann et al., 1990). The detection limit was 0.5 µg C L^{-1} d^{-1} in the centrifuged brine.

The remaining brine sample was fixed with glutaralderhyde (final concentration 0.1% and 2.5%, respectively) for bacterial and microalgal abundance determination. Samples for bacterial abundance were stored at -80 °C for six months until analysis. Bacteria were stained with SYBR Green Nucleic Acid Gel Stain (Invitrogen) for 10 minutes in darkness. Counting was performed with a FACSCanto II flowcytometer (BD Biosciences, Mountain View, USA) and FACSDiva software (BD Biosciences). Flow was determined with an internal standard of fluorescent microspheres (Ø = 1µm). Concentration of the internal standard was determined by triplicated measurement together with BD Trucount Controls. For microalgal cell density,

1-5 mL of a well-mixed sample (brine) was counted in a Sedgewick Rafter counting chamber, and counting and species identification were performed using light microscopy.

Quantification of all biological parameters may have been under-estimated due to the fact that we chose to make the measurements in brine collected after centrifugation. There is a risk that both algae and bacteria attached to surfaces remain within the ice matrix, although this is more probable for large algal cells, and it is known that only 80 % of the total brine volume could be extracted (Eicken et al., 2000). Centrifugation of the ice cores was still judged to be the best sampling technique for this study, considering the low temperature of the sampled ice and the risk for algae and bacteria to be exposed to both osmotic and thermal shock if the ice would have been melted before analysis.

For radiation measurements, a PMA2100 radiometer equipped with a 2π PMA2132 sensor (Solar Light, Philadelphia, USA) was used to record photosynthetic photon flux (PPF) at 400-700 nm (corresponding to photosynthetic active radiation (PAR)) on the docks of Ny-Ålesund, i.e. 500 m from the experimental site. In addition, PPF was measured in ice with a spherical sensor (QSL-2100, id 1.25 cm, Biospherical Instruments Inc., San Diego, USA). To avoid shading from the instrument, the sensor was deployed at 45° angle through the ice.

2.6 Statistical analysis

Simca 12.0.1 (Umetrics, Umeå, Sweden) was used for orthogonal partial least squares discriminant analysis, OPLS-DA, modeling (Bylesjö et al., 2006). In OPLS-DA, a regression model is calculated between the data and a response variable that only contains class information. Consequently, a single component is used as the predictor of a class. The other component describes the variation orthogonal to the predictive component. The predictive component describes the differences between the average values of two classes, in our case,

the control samples and the newly frozen ones. The OPLS-DA will increase class separation, and for a two class problem one predictive component will be calculated.

All data (observations) from the melted ice cores was used in the statistical analysis, although some samples were excluded due to sediment contamination (see result section). The variables (loading factors) used were the halocarbon compounds listed in section 2.4, temperature, bulk salinity, estimated brine volume and the biology data described in section 2.5. All values were scaled with unit variance (UV) prior to modelling, which gives equal weight to all variables. The model was evaluated by Q^2 and R^2X, where Q^2 is a measure of the quality of the model based on cross-validation, where fractions of data are systematically kept out. Q^2 is a sum of squares that is accumulated for the deviations from the actual model response y. The Q^2 values are calculated per model component and can be reported as a cumulative value for the determined number of components. In principle, R^2X is the same measure but without cross validation. For OPLS, R^2X of the predictive component is also a measure of how much of the variation in X that is related to the variation in Y.

3. Results

3.1 Statistical analysis, co-variation of halocarbons

An orthogonal partial least squares discriminant analysis (OPLS-DA) was used to evaluate if the newly formed ice (class 1) was significantly different compared to the control ice (class 2). This multivariate technique can be used when two categories (classes) of observations are tested, to find what distinguishes between them (see section 2.6). The major difference found between the control and the newly frozen ice, was that newly formed ice was enriched in brominated halocarbons relative to iodinated ones, while the iodinated halocarbons were more enriched than brominated ones in the control ice (Figure 2). The highest concentrations of brominated halocarbons in newly formed ice could be found in the upper most layers (0-10

cm). The lower most parts of the newly formed ice were more similar to the control ice. Also, it was seen from the location of bacterial abundance on the right side of the loading plot that it contributed to the observed difference between the classes, with somewhat higher abundances found in the newly frozen ice. Temperature, brine volume and salinity did not influence the separation between classes to any higher degree.

The OPLS-DA model also revealed that many of the measured halocarbons co-varied. The strongest relations were found between the brominated substances $CHBr_3$, $CHBr_2Cl$, $CHBrCl_2$ and CH_2Br_2. In addition the iodinated substances 1-C_3H_7I and CH_2I_2 co-varied with the brominated ones. We have chosen to present vertical distributions of two selected substances as representatives of iodinated and brominated compounds, CH_2ClI and $CHBr_3$. The distribution of CH_2BrI differed from the others, and is also shown in the results (Figure 3 and Figure 4).

3.2 Concentration and distribution of halocarbons in sea ice

During freezing, dissolved ions and gases are excluded from the ice matrix and concentrated in the sea ice brine (Richardson, 1976). The measured bulk halocarbon concentrations (concentration in melted ice) must therefore be divided by brine volume fraction (see section 2.4) to estimate the halocarbon concentration in the brine. When we compared the brine corrected values to brine concentrations measured directly in the brine samples, we generally found a good agreement, which showed that halocarbons were in fact dissolved in the liquid phase. Median concentrations of the predominantly biogenic halocarbons $CHBr_3$, CH_2Br_2, $CHBrCl_2$, $CHBr_2Cl$, CH_2ClI and CH_2BrI in brine and sea ice, were higher than mean concentrations in seawater (Table 1).

3.2.1 Newly frozen ice

In the newly frozen ice, there were large differences in vertical distribution and concentration changes with time between the three halocarbons: $CHBr_3$, CH_2ClI, and CH_2BrI, chosen to represent halocarbon variation (see section 3.2, Figure 3). For $CHBr_3$ the highest concentrations were found in the two uppermost layers of the ice. $CHBr_3$ had a concentration increase in the surface of the freezing ice with time, and 270 pmol L^{-1} (brine volume corrected concentration) was measured on experimental day 12. A similar depth distribution and increase was seen for the other brominated compounds $CHBr_2Cl$, $CHBrCl_2$ and CH_2Br_2 (data not shown). A concentration increase in the surface was also observed for the iodinated compounds ethyliodide, 1-iodopropane, 2-iodopropane and 1-iodobuthane (data not shown).

CH_2BrI on the other hand, had a steadily decreasing concentration at all depths. In the surface ice it decreased from the initial 8.0 pmol L^{-1} to 2.6 pmol L^{-1} after 12 days. CH_2BrI was the only compound that had a clearly decreasing concentration with time in the freezing ice. The concentration of CH_2ClI varied between 2.1 and 8.2 pmol L^{-1} in the new ice and the highest concentrations were often found on 7.5 cm depth. A similar depth distribution was observed for 1-iodopropane and 2-iodopropane (data not shown). For CH_2ClI there was no clear trend with time, but occasional samples were found, at all depths, with a concentration that was 1-2 pmol L^{-1} higher than in the surrounding ice and this was also reflected in a majority of the other iodinated compounds (data not shown).

3.2.2 Control ice

The brine volume corrected concentrations of $CHBr_3$, CH_2ClI and CH_2BrI in the control samples, i.e. from old ice, were generally lower than in the newly frozen ice and more evenly distributed vertically (Figure 4). On experimental days 1 to 9, CH_2BrI and CH_2ClI had higher concentrations at 12 to 22 cm depth in the ice than above and below. Concentrations of all three halocarbons were generally higher on the last two experimental days than in the

beginning of the experiment. The changes with time in physical parameters (Figure 4d-f) were not well reflected in halocarbon concentrations in the control ice (Figure 4a-c).

3.2.3 Sediment inclusion in sea ice

A feature that was seen in halocarbon depth distribution plots for control ice and for CH_2BrI and CH_2ClI in newly frozen ice (Figure 3a-c and 3a-c) was increasing halocarbon concentrations in the lowest part of the ice on the last 3 days of the experiment. This resulted from the ice being in contact with bottom sediment, which contained organic material and most likely bacteria. Since the experimental site was a shallow bay with strong tides the bottom ice was sometimes in contact with the sediment and traces of particles and macro algae were found in some of the ice samples. Sediment was also found in some control ice samples on experimental days 5 to 9. Here, the halocarbon concentrations were higher, up to 10 times that of the other samples. These samples (4 samples in new ice and 10 in control ice) were excluded in all tables and figures. Although samples with very high halocarbon concentrations containing sediment were removed from the results, influence from sediment, which caused an increase in concentration in overlying ice, was likely.

3.3 Microbiological abundance and activity in newly frozen and control ice

In our experiment, algal abundance in newly formed ice was too low for quantification until experimental day 8. On experimental days 8 and 10 microalgal abundance in the new ice varied between 14×10^4 and 42×10^4 cells L^{-1} brine and could only be quantified in the bottom 5 cm. In the control ice, microalgae were quantifiable in all bottom ice samples, but not in the overlying ice, and the abundances varied between 7.1×10^4 and 8.8×10^5 cells L^{-1} brine with no obvious trend with time. The most frequently occurring microalgal genera belonged to the pennate diatoms *Synedropsis* sp., and *Fragilariopsis* sp., typical for ice-algal communities.Maximum quantum yield of photosynthesis (F_v/F_m) could only be measured in

322 the lower parts of newly frozen and control ice. In the newly formed ice, F_v/F_m could first be
323 measured on day 5 and varied between 0.06 and 0.42. In control ice it ranged between 0.06
324 and 0.50 (Figure 5).

325 There was a standing stock of heterotrophic bacteria in both the control and newly frozen
326 ice with bacteria present in all ice samples. No evident vertical distribution of bacteria was
327 observed, and the bacterial abundance ranged between 4.7×10^4 and 8.1×10^5 cells mL^{-1} brine
328 in newly frozen ice brine and 7.1×10^4 and 6.4×10^5 cells mL^{-1} in the control ice (Figure 5).
329 Bacterial producion (BP) was measured in centrifuged brine, and many of the measurements
330 were below the detection limit of the method (0.5 µg C L^{-1} d^{-1}), which meant that we could
331 not measure BP at levels as low as have been found in other investigations (Søgaard et al.,
332 2010). In newly frozen ice, BP could be quantified in 11 out of 36 samples and ranged
333 between 0.5 and 11 µg C L^{-1} d^{-1}. The highest production rates, 10 and 11 µg C L^{-1} d^{-1}, were
334 found in the surface ice on experimental day 5 and on day 8 at 17.5 cm depth. In the control
335 ice, BP was high enough to be quantified in 7 out of 29 samples, and the range was 0.5 to 9.1
336 µg C L^{-1} d^{-1}. The highest values of BP were detected on day 8 at 17.5 and 27.5 cm depth.

337 *3.4 Frost flowers*

338 While the freezing experiment was running, new sea ice was formed further out in the bay,
339 200 m from our study site, and frost flowers were formed. Frost flowers are crystalline
340 structures that form on new sea ice when air, which is supersaturated with water vapor,
341 condenses at the ice surface. Brine that forms at the ice surface is wicked up by the ice
342 skeleton through the effects of surface tension and concentration gradients (Abbatt et al.,
343 2012). Frost flowers have been attributed as one of the sources of inorganic bromine to the
344 atmosphere in Polar Regions. Since they exhibit high salinities and high bromide
345 concentrations they are believed to be a part of the formation of Br_2 and HOBr, which

346 ultimately participate in the destruction of ozone (Kaleschke et al., 2004 and references there
347 in). However, the contribution of organo-bromine from frost flowers has not been addressed.
348 The frost flowers were sampled (duplicate) when they were newly formed, and again 20
349 hours later (one sample). A relatively high concentration of $CHBr_3$, 51 and 66 pmol L^{-1} was
350 found in the new frost flowers. This concentration was comparable to the brine concentration
351 of $CHBr_3$ of 47 pmol $L^{-}1$ on that specific day, and higher than the under ice water
352 concentration of 18 pmol L^{-1}. The same relationship was seen for $CHBrCl_2$ and $CHBr_2Cl$
353 (Table 1, Table 3). CH_2ClI and CH_2BrI were also detected in the new frost flowers, but in
354 lower concentrations than in brine, and the frost flower concentrations were in the same range
355 as in under ice water and seawater (Table 1). When the frost flowers from the same location
356 were sampled 20 hours later, all measured halocarbon concentrations were lower, and
357 approximately 95% of the halocarbon content had disappeared. In contrast, the salinity, 52 in
358 new frost flowers and 53 in old, did not change, indicating that processes other than salinity
359 changes affected the halocarbon concentrations (Table 3).

360 **4. Discussion**

361 The results from this freezing experiment were intended to mimic sea ice freezing from
362 natural seawater in an environment as natural as possible in terms of irradiation, air
363 temperatures and biological parameters. There were, however, drawbacks with the
364 experimental design where water froze in bore holes, such as faster freezing of the ice than
365 normally, and that the ice froze both downwards and inwards. This was reflected in the
366 temperature of the newly frozen ice, which mimicked the temperature of the surrounding ice,
367 and at the first six experimental days, the lower parts of the ice were colder than would
368 normally be expected. Also, this inward growth had a negative effect on the porosity of the
369 newly formed ice, meaning it had no upper frazil layer and a less pronounced columnar

downward growth than normal new sea ice. This less porous ice probably had a smaller brine volume and a slower transport through brine channels than naturally formed sea ice. The experiment still gave us an insight in events during freezing of natural seawater, with the complicated connections between physical and biological processes and their effects on halocarbon concentrations in the ice. Below follows a process discussion based on our measurements.

4.1 Ice physical effects

In our results we present halocarbon concentrations in sea ice brine. Those concentrations are affected by the physical concentration and dilution of the brine that is caused by temperature changes in the ice. Lower temperatures will result in a smaller brine volume and more saline, concentrated brine and vice versa. If halocarbon concentrations in brine in the sampled ice are compared to the physical parameters, it is seen that variations in halocarbon concentrations in brine cannot be explained exclusively by temperature, salinity and brine volume (Figure 3 and Figure 4). The physical concentration and dilution effects in the brine are, thus, not the only factors that determine halocarbon concentration in our study.

The new ice, and to a smaller extent the control ice, was affected by brine drainage where brine migrated downward due to gravity and natural convection. It is also possible that brine was expulsed upwards due to decreasing temperatures. These brine effects resulted in a decrease in bulk salinity, and also a decrease in bulk halocarbon concentration, but did not directly affect halocarbon concentrations in the remaining brine.

4.2 Biotic and abiotic processes

Except for CH_2BrI in the new ice, local high concentrations and local concentration increases of halocarbons, were found in both newly frozen and control ice during the study. A plausible explanation for this is biological halocarbon production that occurred locally in the

ice (Figures 3a-c and 4a-c). Halocarbons are known to be formed by ice algae during photosynthesis through the scavenging of hydrogen peroxide by haloperoxidases (Manley, 2002). There is also a possibility that halocarbons were produced by heterotrophic bacteria since hydrogen peroxide is formed during respiration, and thereby halocarbons can be formed. There are few reports of bacterial halocarbon production, but for example CH_3I production has been related to bacterial aggregates (Asare et al., 2012) and cyanobacteria, have been linked to production of $CHBr_3$, CH_3I, CH_2Br_2 and $CHBr_2Cl$ (Karlsson et al., 2008).

Bacterial Production (BP) in new and control ice was detected in too few samples to determine if they were linked to variations in halocarbon concentrations. Maximum BP in the control ice was observed on day 8 and on days 5 and 8 in the newly frozen ice. Elevated concentrations of CH_2ClI and $CHBr_3$ were observed at 0 to 10 cm depth in the newly frozen ice on days 5 and 8, but maximum BP was found at 17.5 cm depth and a relation could not be determined. Unfortunately halocarbon measurements for the control ice on day 8 failed due to instrumental problems.

The vertical distribution of algae and heterotrophic bacteria, with micro algae found only in the bottom ice, and bacteria more evenly distributed vertically in the ice, may indicate that bacteria were in fact responsible for the local increases in halocarbon concentrations in new and old ice, since these increases were mainly found in the middle or upper layers of the ice. A weak positive correlation was found between bacterial abundance and CH_2BrI in control ice, which implies a bacterial production of this compound in the old ice (Spearman's rank correlation, ρ=0.38, p= 0.09, n=20), but this was not found for the other halocarbon compounds and not in the newly frozen ice. Microalgal and bacterial abundances in our study were of the same magnitude as other measurements made in winter sea ice (Junge et al., 2002; Arrigo et al., 2010). However, because of the high detection limit for the microbial analysis

418 (see section 2.5) we may have overlooked low concentrations of micro algae or bacteria that
419 would have been useful for the interpretation of our results.

420 Our interpretation of the different distributions of the three halocarbons in newly frozen
421 sea ice is that CH_2ClI and $CHBr_3$ were produced in the sea ice during the experiment, but
422 CH_2BrI was not. Thus, our findings suggest that halocarbons are produced by
423 microorganisms in newly frozen sea ice even in the early spring, before the spring bloom. For
424 the control ice the changes with time in the physical parameters (Figure 4d-f) were not well
425 reflected in halocarbon concentrations (Figure 4a-c), and the most pronounced changes in
426 halocarbon concentrations in the control ice were probably caused by biological production
427 and influence from sediment inclusions. Our findings indicate coastal sediment as a possible
428 source of halocarbons, although we had no possibility to follow up these results in this study.

429 During the study decreases in halocarbon concentrations were seen, in particular for
430 CH_2BrI in the newly frozen ice (brine corrected concentration). The causes for this decrease,
431 besides the physical dilution of brine, could be photolysis, microbial degradation or diffusion
432 of CH_2BrI to air and water. Photolysis in the surface ice of iodinated halocarbons is a fast
433 process and happens in the timescale of hours to minutes (Ordóñez et al., 2012). This
434 degradation process is therefore not likely to be the reason for the slower changes in
435 halocarbon concentrations that were seen in this study. A not so well investigated process is
436 the microbial degradation of halocarbons, and we cannot exclude this as a removal process in
437 our study. However, a study of the correlation between bacterial abundance and the measured
438 halocarbons with Spearman's rank correlation did not result in any negative correlations
439 between bacterial abundance and halocarbons. We therefore chose to investigate further if
440 there was a diffusive flux of halocarbons from the newly frozen ice.

441 *4.3 Rates of halocarbon production and removal*

To investigate if we had a diffusive flux of halocarbons from the ice to the atmosphere during freezing, the mean concentration of the top 10 cm (whole core for day 1) of the newly frozen ice and the control ice were assessed as a function of time. We assumed that in the top layers of the ice there was no influence on the concentrations from underlying sediment. In order to exclude the effects on halocarbon concentrations due to brine concentration and dilution effects, the bulk halocarbon concentrations were normalized to salinity (divided by bulk salinity) (Figure 6). A salinity normalized data plot, will reveal changes in halocarbon concentrations that are due to chemical and biological processes.

For $CHBr_3$ in newly frozen ice, we observed time periods of increase (day 1 to day 3) and decrease (day 3 to 6 and day 7 to 10) (Figure 3a and Figure 6). We interpreted these as periods where either biological production or removal dominated. Using the salinity normalized increase, we could estimate the net production rate 14 pmol L^{-1} d^{-1} from day 1 to 3 for bromoform, and the salinity normalized decrease, where diffusive transport and/or degradation dominated, was used to estimate the net removal rate, 12 and 18 pmol L^{-1} d^{-1} from day 3 to 6 and day 7 to 10 respectively. These rates can be compared to the estimated net production rates of 0 to 19 pmol L^{-1} d^{-1} for brominated compounds from incubations of brine from Antarctic sea ice (Mattsson et al., 2012). The concentration changes of CH_2ClI with time could not be used for production or degradation estimates since none of the processes dominated during the study (Figure 6).

4.4 Diffusion of halocarbons to air

A combination of processes may have caused decreases in halocarbons in the newly frozen ice, but as discussed in section 4.3, diffusion from brine channels to the overlying air was probably the most important of those. When the brine volume is below 5 %, which is the case for the studied ice on the coldest days of the experiment, columnar ice becomes impermeable

466 to fluids (Golden et al., 1998), but it is not known when sea ice becomes impermeable to
467 gases. Considering the evolution of gas concentration in newly formed sea ice with time,
468 Mock et al. (2002) concluded that as sea ice becomes older, the result is degassing of the ice,
469 and the gases that were expelled from the forming ice matrix, and dissolved in the liquid
470 brine, are ultimately released to the atmosphere or to the underlying water.

471 It has been suggested that the diffusive gas flux through sea ice is mediated by gas
472 bubbles. Such bubbles could either be trapped in the ice during freezing, or formed during
473 photosynthesis by ice algae (Mock et al., 2002). Diffusion rates in sea ice for oxygen and SF_6
474 determined by Loose et al. (2011) were dependent not only on ice temperature and porosity of
475 the ice, but also on the partition of the gas to bubbles and were, thus, faster than liquid
476 diffusion. If this is true for our samples, we should be able to observe a transport to air from
477 the newly frozen ice. The recent studies by Loose et al. (2010) and Shaw et al. (2011) suggest
478 that halogenated gases dissolved in liquid brine are transported to the atmosphere through
479 diffusion in the ice, with diffusion constants (D) on the order of 10^{-5} to 10^{-4} cm^2 s^{-1}.

480 For the halocarbon compounds that were produced in the ice during the study the
481 potential transport to air was difficult to detect. However, in absence of production, as was the
482 case for CH_2BrI in new ice, a concentration decrease with time was observed that may have
483 been caused by a diffusive transport to air. The salinity normalized data plot for CH_2BrI
484 shows a decrease in surface concentration the first nine days of the experiment that was not
485 seen in the control ice. The non-conservative behavior of CH_2BrI relative to salinity in the
486 new ice (Figure 6) demonstrated that desalination alone was not responsible for the removal
487 of CH_2BrI. The maximum concentration of CH_2BrI was found on 7.5 cm depth. If we assume
488 that upward diffusion was the only process causing concentration decrease at this depth, we
489 can calculate the diffusion coefficient of CH_2BrI with Fick's first law:

$$F = -D\frac{dC}{dz} \quad (1)$$

Where F = flux (pmol cm^{-2} s^{-1}), D = diffusion coefficient for the specific compound (cm^2 s^{-1}) and $\frac{dC}{dz}$ = upward concentration gradient from maximum concentration (pmol cm^{-4}).

The flux was estimated from the decrease in salinity normalized concentrations from 7.5 cm depth during the first nine experimental days by using the volume and surface of the ice core section and corresponded to a contribution of 3 pmol CH_2BrI per m^2 ice per day. The mean gradient to the surface ice from 7.5 cm depth during the same period was used as the upward concentration gradient. These calculations resulted in D = 7.5 x 10^{-5} (cm^2 s^{-1}) for CH_2BrI, which is in good agreement with the studies by Loose et al. (2010) and Shaw et al. (2011).

The measured halocarbon concentrations were results of both production and degradation, and their increase or decrease depended on which process that dominated. It is most likely that the same process or processes that caused depletion of CH_2BrI in the sea ice during freezing, also affected the other halocarbons. The fact that CH_2ClI and $CHBr_3$ did not show a concentration decrease in the salinity normalized graph may be explained by the biological production of these compounds in the ice during our experiment.

The fact that the control ice had a lower average halocarbon concentration, and a more homogenous distribution than the newly frozen ice (Figure 3a-c and 4a-c), indicated that a degassing already had taken place, and that an equilibrium with air had been reached.

4.5 Frost flowers

After frost-flower formation, the lifetime of the frost flowers at the sampling site was observed to be approximately 48 hours. If all the halocarbon content of the frost flowers

512 eventually evaporated, the brominated halocarbons (CH_2Br_2, $CHBr_2Cl$, $CHBrCl_2$ and
513 $CHBr_3$) would give a small contribution of 300 pmol m^{-2} to the atmospheric bromine. If we
514 assume a shallow inversion layer of 100 m (Mickle et al., 2012), the contribution to the
515 atmospheric boundary layer would be approximately 0.07 pptv Br. The measured mixing
516 ratios of bromoform (0.45 – 32 pptv) in the Arctic have been reviewed by Quack and Wallace
517 (2003), and in the lower end of this range frost flowers may have an impact on local air
518 concentrations of brominated halocarbons. Since halocarbons are easily evaporated, frost
519 flowers form an efficient transport path for halocarbons from ice to atmosphere, although of
520 short duration.

521 **Conclusions**

522 Concentration and distribution of halocarbons in sea ice were found to be governed by
523 competing processes: removal processes and production in the ice which may have been
524 caused by ice-living organisms. The concentration changes with time, thus, depended on the
525 process that dominated. Biological production was found to be the most likely process for
526 local increases in halocarbon concentrations in new and old ice. We could not establish a
527 correlation between the measured biological parameters and halocarbon concentrations, but
528 the vertical distribution of bacteria, algae and halocarbons may suggest a bacterial halocarbon
529 production.

530 Our results indicated that halocarbons were removed from young sea ice by processes
531 other than desalination. Concentration gradients in the surface ice on the first days of the
532 experiment may have been caused by a diffusive transport from the surface ice to the
533 atmosphere. The decrease rates were faster than desalination of the ice and in good agreement
534 with the rate of a diffusive transport. However, chemical or biological degradation causing
535 halocarbon concentration decrease could not be ruled out. Further studies of diffusion and

transport through natural sea ice are needed to determine the potential strength of this halocarbon source to the atmosphere.

Bottom ice halocarbon concentrations indicated an exchange between sea ice brine channels in the bottom ice and underlying water and sediment, and halocarbon concentrations were higher in sea ice after contact with bottom sediment. Future research should investigate sediment as a potential halocarbon source.

Frost flowers on new sea ice were shown to be enriched in several halocarbons, and the frost flower concentrations of these compounds were similar to concentrations in sea ice brine. They are, thus, an additional transport of organo-halogens to the atmosphere, although their contribution is probably minor and of short duration.

Acknowledgements

This is a contribution to the project “Greenhouse gases and Mercury in a changing Arctic”, funded by the Swedish Research Council (#2007-8365). We would like to thank two anonymous reviewers for their help to improve this manuscript.

References

Abbatt, J. P. D., J. L. Thomas, K. Abrahamsson, C. Boxe, A. Granfors, A. E. Jones, et al., 2012. Halogen activation via interactions with environmental ice and snow in the polar lower troposphere and other regions, Atmospheric Chemistry and Physics, 12(14), 6237-6271, doi: 10.5194/acp-12-6237-2012.

Arrigo, K. R., T. Mock, and M. P. Lizotte, 2010. Primary Producers and Sea Ice, in Sea Ice, Second Edition, edited by D. N. Thomas and G. S. Dieckmann, Blackwell Publishing Ltd.

Asare, N. K., C. M. Turley, P. D. Nightingale, and M. Nimmo, 2012. Microbially-mediated methyl iodide production in water samples from an estuarine system, Journal of Environment, 01(03), 75-83.

Bylesjö, M., M. Rantalainen, O. Cloarec, J. K. Nicholson, E. Holmes, and J. Trygg, 2006. OPLS discriminant analysis: combining the strengths of PLS-DA and SIMCA classification, Journal of Chemometrics, 20(8-10), 341-351, doi: 10.1002/cem.1006

564 Carpenter, L. J. and P. S. Liss, 2000. On temperate sources of bromoform and other reactive
565 organic bromine gases, J. Geophys. Res., 105(D16), 20539-20547, doi:
566 10.1029/2000JD900242.
567 Collén, J., A. Ekdahl, K. Abrahamsson, and M. Pedersén, 1994. The involvement of hydrogen
568 peroxide in the production of volatile halogenated compounds by Meristiella gelidium,
569 Phytochemistry, 36(5), 1197-1202, doi: 10.1016/S0031-9422(00)89637-5.
570 Eicken, H., C. Bock, R. Wittig, H. Miller, and H. O. Poertner, 2000. Magnetic resonance
571 imaging of sea-ice pore fluids: methods and thermal evolution of pore microstructure,
572 Cold Regions Science and Technology, 31(3), 207-225, doi: 10.1016/s0165-
573 232x(00)00016-1
574 Ekdahl, A., M. Pedersén, and K. Abrahamsson, 1998. A study of the diurnal variation of
575 biogenic volatile halocarbons, Mar Chem, 63(1-2), 1-8, doi: 10.1016/S0304-
576 4203(98)00047-4
577 Frankenstein, G., and R. Garner, 1967. Equations for determining the brine volume of sea ice
578 from -0.5°C to -22.9°C, Journal of Glaciology, 6(48), 943-944.
579 Golden, K. M., S. F. Ackley, and V. I. Lytle, 1998. The Percolation Phase Transition in Sea
580 Ice, Science, 282(5397), 2238-2241.
581 Jones, A. E., P. S. Anderson, E. W. Wolff, J. Turner, A. M. Rankin, and S. R. Colwell, 2006.
582 A role for newly forming sea ice in springtime polar tropospheric ozone loss?
583 Observational evidence from Halley station, Antarctica, J. Geophys. Res., 111(D8),
584 D08306, doi: 10.1029/2005JD006566
585 Junge, K., F. Imhoff, T. Staley, and J.W. Deming, 2002. Phylogenetic diversity of
586 numerically important Arctic Sea.ice bacteriacultured at subzero temperature,
587 Microbial Ecology, 43(3), 315-328, doi: 10.1007/s00248-001-1026-4.
588 Kaleschke, L., et al., 2004. Frost flowers on sea ice as a source of sea salt and their influence
589 on tropospheric halogen chemistry, Geophys. Res. Lett., 31(16), L16114, doi:
590 10.1029/2004GL020655.
591 Karlsson, A., N. Auer, D. Schulz-Bull, and K. Abrahamsson, 2008. Cyanobacterial blooms in
592 the Baltic — A source of halocarbons, Mar Chem, 110(3–4), 129-139, doi:
593 10.1016/j.marchem.2008.04.010.
594 Karlsson, A., 2012. Formation and Distribution of Marine Biogenic Halocarbons with
595 Emphasis on Polar Regions, Ph.D. Thesis, University of Gothenburg, Gothenburg,
596 Sweden.
597 Lee, S., and J. A. Fuhrman, 1987. Relationship between biovolume and biomass of naturally
598 derived marine bacterioplankton, Applied and Environmental Microbiology, 536,
599 1298-1303.
600 Loose, B., P. Schlosser, D. Perovich, D. Ringelberg, D. T. Ho, T. Takahashi, J. Richter-
601 Menge, C. M. Reynolds, W. R. McGillis, and J. L. Tison, 2011. Gas diffusion through
602 columnar laboratory sea ice: implications for mixed-layer ventilation of CO2 in the
603 seasonal ice zone, Tellus B, 63(1), 23-39, doi: 10.1111/j.1600-0889.2010.00506.x.
604 Manley S. L., 2002. Phytogenesis of halomethanes: Aproduct of selection or a metabolic
605 accident? Biogeochemistry, 60(2), 163-180, doi: 10.1023/a:1019859922489.
606 Mattsson, E., A. Karlsson, W. O. Smith, and K. Abrahamsson, 2012. The relationship
607 between biophysical variables and halocarbon distributions in the waters of the
608 Amundsen and Ross Seas, Antarctica, Mar Chem, 140-141, 1-9, doi:
609 10.1016/j.marchem.2012.07.002.
610 Mickle, R.E., Bottenheim, J.W., Leaitch, W.R. and Evans, W., 1989. Boundary layer ozone
611 depletion during AGASP-II. Atmospheric Environment, 23(11): 2443-2449.
612 Mock, T., G. S. Dieckmann, C. Haas, A. Krell, J. L. Tison, A. L. Belem, S. Papadimitriou,
613 and D. N. Thomas, 2002. Micro-optodes in sea ice: A new approach to investigate

614 oxygen dynamics during sea ice formation, Aquatic Microbial Ecology, 29(3), 297-
615 306.
616 Ordóñez C, J.-F Lamarque, S. Tilmes, D. E. Kinnison, E. L. Atlas, D. R. Blake, G. Sousa
617 Santos, G. Brasseur, and A. Saiz-Lopez, 2012. Bromine and iodine chemistry in a
618 global chemistry-climate model: description and evaluation of very short-lived oceanic
619 sources, Atmos. Chem. Phys.,12, 1423-1447, doi: 10.5194/acp-12-1423-2012
620 Quack, B., and D. W. R. Wallace, 2003. Air-sea flux of bromoform: Controls, rates and
621 implications, Global Biogeochemical Cycles, 17(1), 1023,
622 doi:10.1029/2002GB001890, 2003.
623 Richardson C., 1976. Phase relationships in sea ice as a function of temperature, Journal of
624 Glaciology, 17, 507–519.
625 Riemann, B., R. T. Bell, and N. O. G. Jörgensen , 1990. Incorporation of thymidine adenine
626 and leucine into natural bacterial assemblages, Marine Ecology Progress Series,
627 65(87-94).
628 Schlitzer, R., Ocean Data View, http://odv.awi.de, 2010.
629 Shaw, M. D., L. J. Carpenter, M. T. Baeza-Romero, and A. V. Jackson, 2011. Thermal
630 evolution of diffusive transport of atmospheric halocarbons through artificial sea–ice,
631 Atmospheric Environment, 45(35), 6393-6402, doi: 10.1016/j.atmosenv.2011.08.023
632 Simpson, W. R., et al., 2007. Halogens and their role in polar boundary-layer ozone depletion,
633 Atmos. Chem. Phys., 7, 4375-4418.
634 Smith, D. C., and F. Azam, 1992. A simple economical method for measuring bacterial
635 protein synthesis rates in seawater using 3H-leucine, Marine Microbial Food Webs, 6,
636 107-114.
637 Sturges, W. T., G. F. Cota, and P. T. Buckley, 1992. Bromoform emission from Arctic ice
638 algae, Nature, 358(6388), 660-662, doi: 10.1038/358660a0.
639 Sturges, W. T., G. F. Cota, and P. T. Buckley, 1997. Vertical profiles of bromoform in snow,
640 sea ice, and seawater in the Canadian Arctic, J. Geophys. Res., 102(C11), 25073-
641 25083.
642 Søgaard, D. H. , M. Kristensen, S. Rysgaard, R.N. Glud, P. J. Hansen, K. M. Hilligsøe, 2010.
643 Autotrophic and heterotrophic activity in Arctic first-year sea ice: seasonal study from
644 Malene Bight, SW Greenland, Marine Ecology Progress Series, 419, 31-45, doi:
645 10.3354/meps08845.
646 Weissenberger, J., G. Dieckmann, R. Gradinger, and M. Spindler, 1992. Sea ice: a cast
647 technique to examine and analyze brine pockets and channel structure, Limnology and
648 Oceanography, 37, 179-183.
649

Figure Captions

Figure 1. Variability of a) photosynthetically active radiation (PAR), b) average wind speed and c) average air temperature (T) during the experiment

Figure 2. Difference between the two classes: control (black) and newly frozen ice (red) as described by an orthogonal partial least squares discriminant analysis, OPLS-DA, model (number of components 1+1, R2X = 0.645, Q2 = 0.419). The score plot (a) clearly shows the separation of the two classes. The ellipse in the score plot indicates the confidence region for a two dimensional plot with the significance level 0.05. The loading plot (b) illustrates the variables separating the two classes. The iodinated compounds represented by filled triangles are:1) 2-iodobuthane, 2) 1-iodobuthane, 3) ethyliodide, 4) 2-iodopropane, 5) methyliodide, 6) chloroiodomethane, 7) bromoiodomethane, 8) 1-iodopropane and 9) diiodmethane. The brominated compounds represented by filled circles are 10) 1,2-dibromoethane, 11) dibromomethane, 12) bromoform, 13) dibromochloromethane and 14) bromodichloromethane. The three halocarbons chosen to represent iodinated and brominated compounds are indicated in red in the loading plot (b).

Figure 3. Halocarbon concentrations and physical variables in new ice during the 12 experimental days: a) $CHBr_3$, b), CH_2BrI c) CH_2ClI, d) ice temperature, e) Bulk salinity and f) Brine volume (v_b/v). Halocarbon concentrations are corrected for brine volume. Variations (in percent of mean halocarbon concentration) between duplicate samples at the same depth were on average 26 % for CH_2ClI, 27 % for CH_2BrI and 17 % for $CHBr_3$. It should be noted that values are interpolated between the sample points. All actual samples are represented by black dots in the graph.

Figure 4. Halocarbon concentrations and physical variables in control ice during the 12 experimental days: a) $CHBr_3$, b), CH_2BrI c) CH_2ClI, d) ice temperature, e) Bulk salinity and

f) Brine volume (v_b/v). Halocarbon concentrations are corrected for brine volume. It should be noted that values are interpolated between the sample points. All actual samples are represented by black dots in the graph.

Figure 5. Maximum quantum yield of photosynthesis (F_v/F_m) and bacterial abundance x 10^4 cells ml^{-1}) in sea ice brine from newly frozen and control ice. It should be noted that values are interpolated between the sample points. All actual samples are represented by black dots in the graph.

Figure 6. Temporal variation of mean halocarbon concentrations in surface ice (0-10 cm depth) normalized to salinity.

Table 1. Halocarbon concentrations and salinities of all samples[a]

Compound	Brine[b] (n=11)	Ice[c] (n=102)	Under-ice water[d] (n=15)	Seawater[e] (n=25)
$CHBr_3$	86 (47-120)	65 (13-270)	18 (11-59)	13 (3.3-25)
CH_2Br_2	28 (27->120)[f]	35 (8.7-150)	14 (4.3-19)	11 (2.6-25)
$CHBrCl_2$	10 (4.0-21)	10.4 (0.71-40)	2.8 (0.38-7.0)	3.1 (0.23-30)
$CHBr_2Cl$	68 (29-150)	53 (4.7-200)	18 (4.6-29)	9.6 (2.7-21)
CH_2BrI	1.8 (0.46-7.0)	2.8 (0.25-8.5)	1.5 (0.84-3.0)	1.0 (0.37-1.8)
CH_2ClI	3.0 (1.2-5.1)	4.1 (0.60-9.2)	1.1 (0.63-2.0	0.81 (0.47-1.0)
CH_2I_2	0.72 (0.44-1.9) (n=6)	2.5 (0.29-11) (n=62)	0.70 (0.17-3.0) (n=9)	0.55 (0.19-1.2) (n=17)
Salinity	120 (91-140)	120 (49-200)	35 (30-39)	34 (34-35)

[a]Samples were collected during the 12 experimental days. Ice samples containing sediment are excluded. Units are in pmol L^{-1} for halocarbons and practical salinity units (psu) for salinity. Ranges are indicated in parenthesis. n = number of observations.

[b]Median halocarbon concentration in brine

[c]Median halocarbon concentration in ice, indicated as concentration in sea ice brine, obtained by dividing bulk ice concentrations by the calculated brine volume (see section 2.4). One sample represents one 5-cm ice core section. Salinity is given as bulk salinity divided by brine volume.

[d]Median halocarbon concentration in under-ice water.

[e]Mean halocarbon concentration in seawater. Samples were collected 500 m from experimental site.

[f]Seven samples were out of instrumental range.

Table 2. Halocarbon concentrations and salinities of melted frost flowers[a]

Compound	Sampling 1[b] (n=2)	Sampling 2[c] (n=1)
$CHBr_3$	51, 66	2.1
CH_2Br_2	3.0, 5.2	0.71
$CHBrCl_2$	6.7, 5.5	0.13
$CHBr_2Cl$	52, 56	0.66
CH_2BrI	0.33, 0.53	0.019
CH_2ClI	0.30, 0.75	0.062
Salinity	51, 52	53

[a] Concentrations are in pmol L^{-1} for halocarbons and practical salinity units (psu) for salinity.

[b] 27 March 2010

[c] 28 March 2010

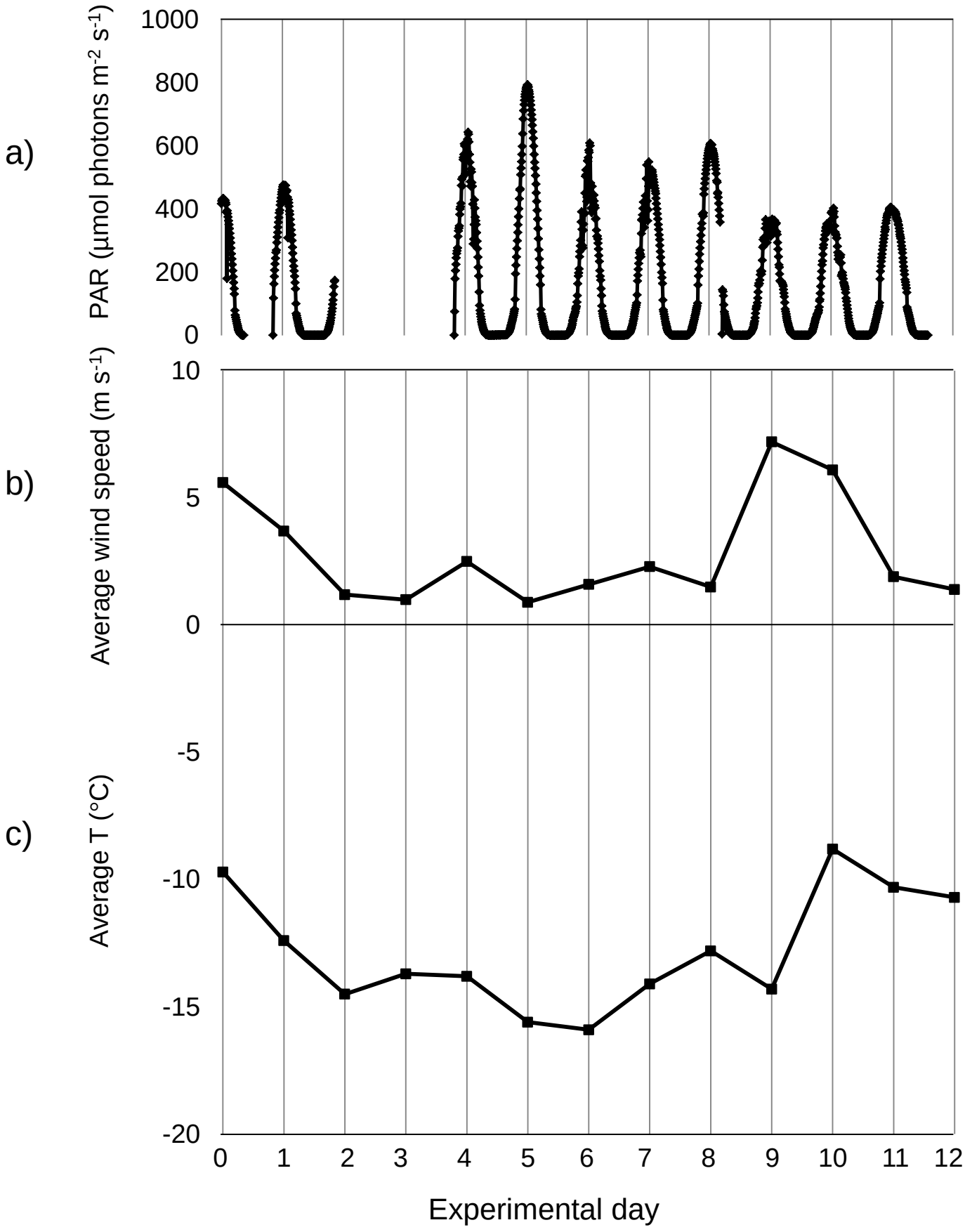
a)
b)
c)
PAR (µmol photons m-2 s-1)
1000
800
600
400
200
0
Average wind speed (m s-1)
10
5
0
Average T (°C)
-5
-10
-15
-20
0
1
2
3
4
5
6
7
8
9
10
11
12
Experimental day

a)

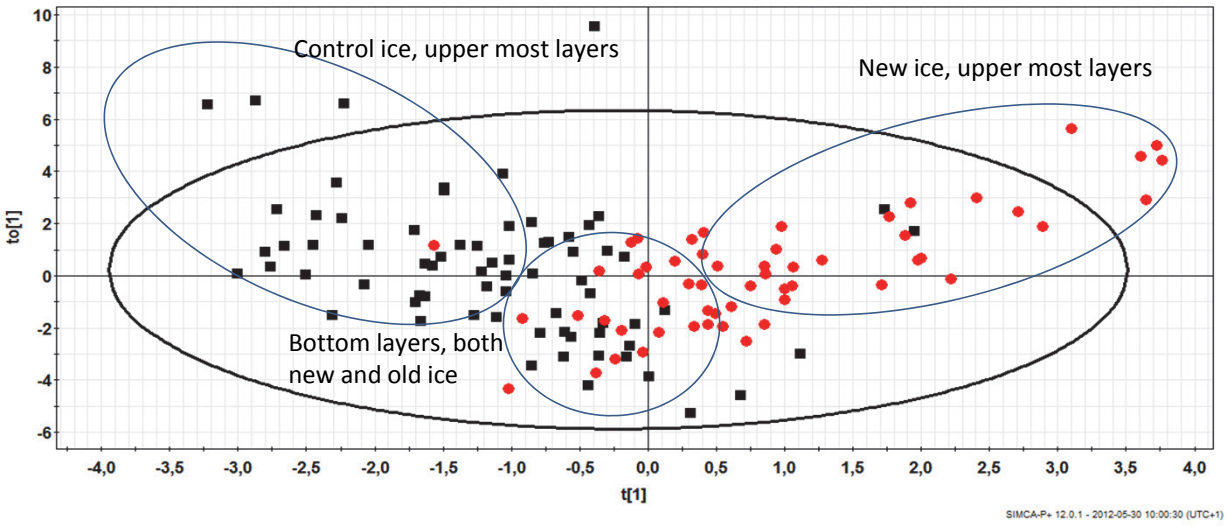
Control ice, upper most layers
New ice, upper most layers
Bottom layers, both
new and old ice
to[1]
t[1]
SIMCA-P+ 12.0.1 - 2012-05-30 10:00:30 (UTC+1)

b)

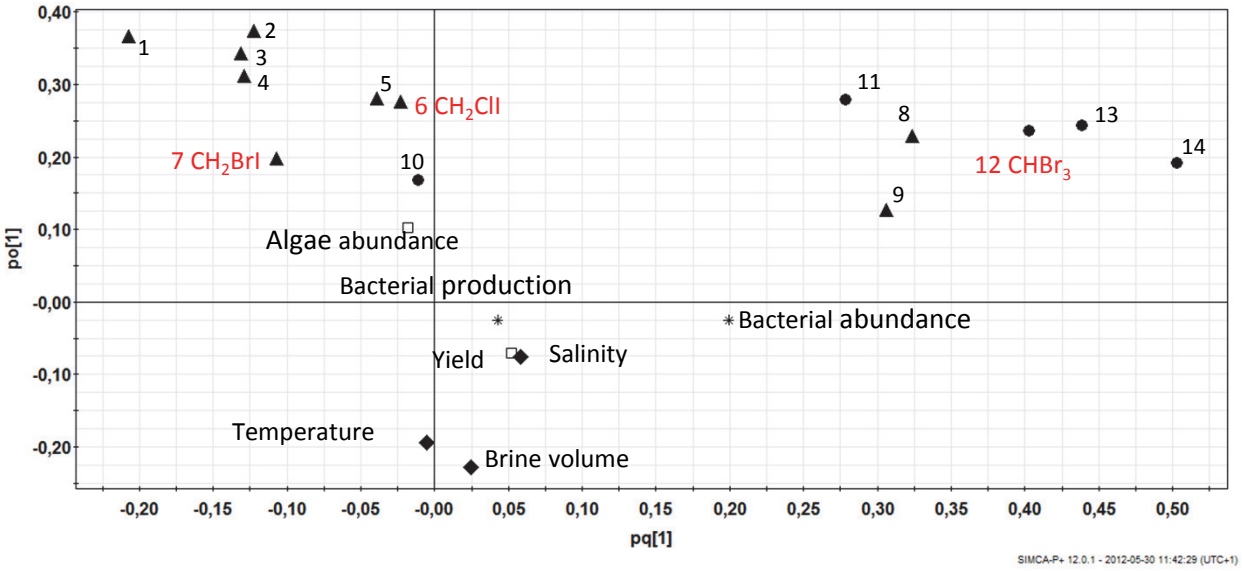
1
2
3
4
5
6 CH2ClI
7 CH2BrI
10
11
8
13
14
12 CHBr3
9
Algae abundance
Bacterial production
Bacterial abundance
Yield
Salinity
Temperature
Brine volume
po[1]
pq[1]
SIMCA-P+ 12.0.1 - 2012-05-30 11:42:29 (UTC+1)

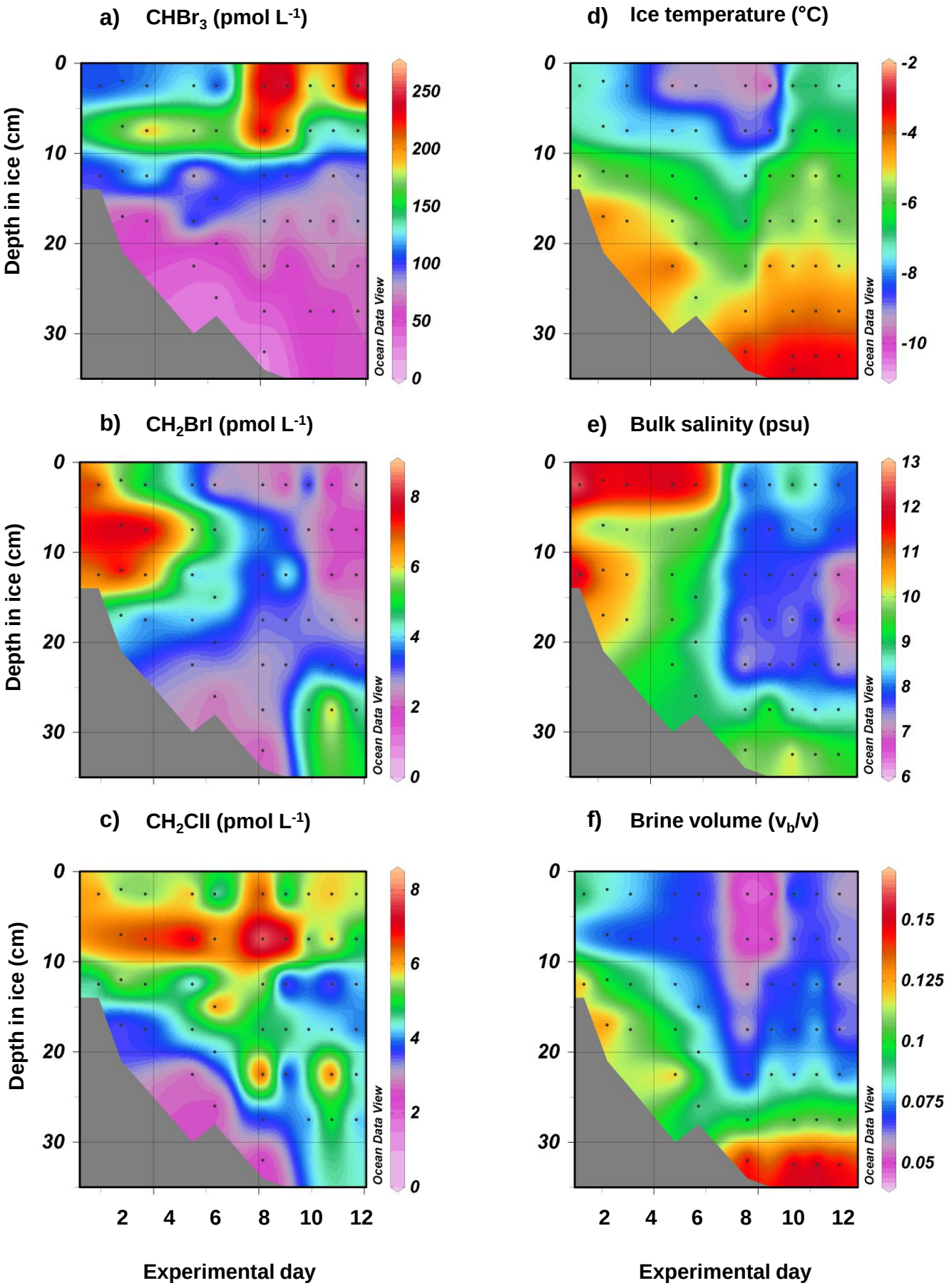
a) CHBr3 (pmol L-1)
d) Ice temperature (°C)
b) CH2BrI (pmol L-1)
e) Bulk salinity (psu)
c) CH2ClI (pmol L-1)
f) Brine volume (vb/v)
Depth in ice (cm)
0
10
20
30
250
200
150
100
50
0
-2
-4
-6
-8
-10
8
6
4
2
13
12
11
10
9
7
0.15
0.125
0.1
0.075
0.05
Ocean Data View
2
4
6
8
10
12
Experimental day

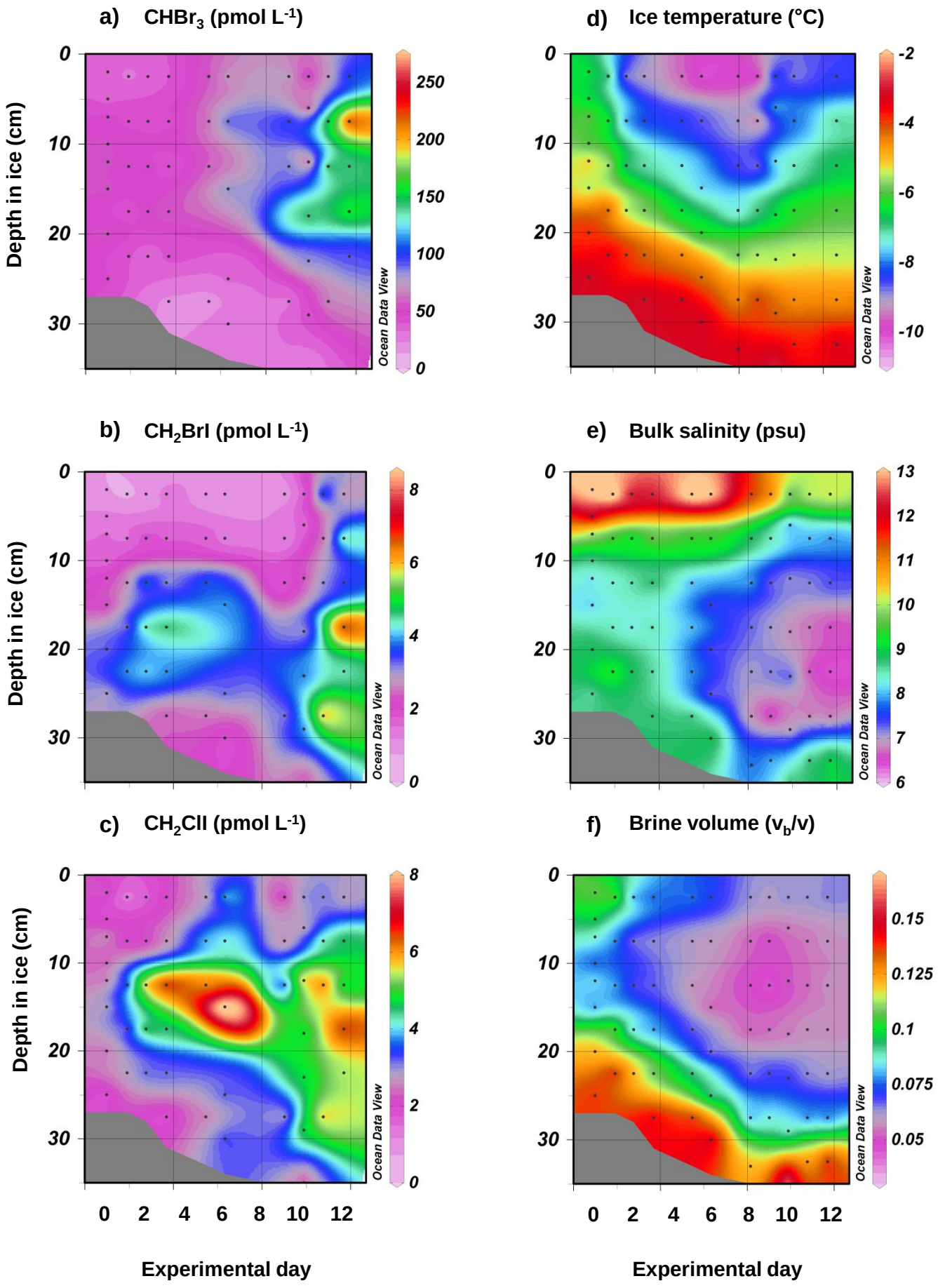
a) CHBr3 (pmol L-1)
d) Ice temperature (°C)
b) CH2BrI (pmol L-1)
e) Bulk salinity (psu)
c) CH2ClI (pmol L-1)
f) Brine volume (vb/v)
Depth in ice (cm)
Experimental day
Ocean Data View

NEWLY FROZEN ICE

Yield (F_v/F_m)

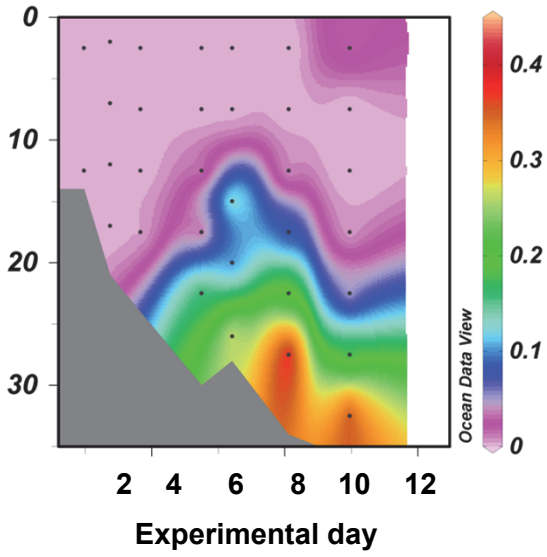

Bacterial abundance (x10^4 cells ml^{-1})

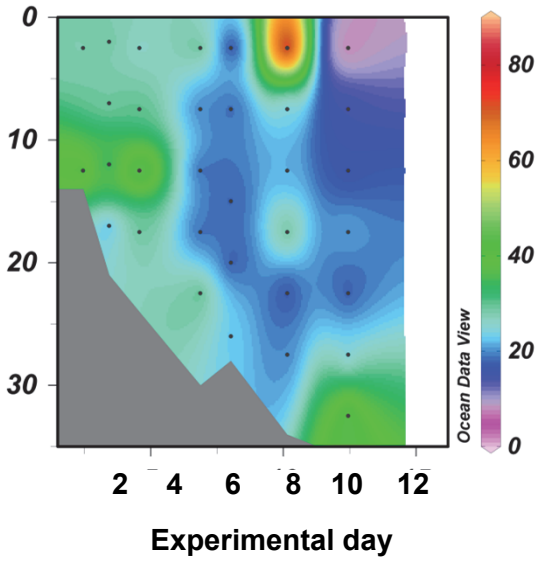

CONTROL ICE

Yield (F_v/F_m)

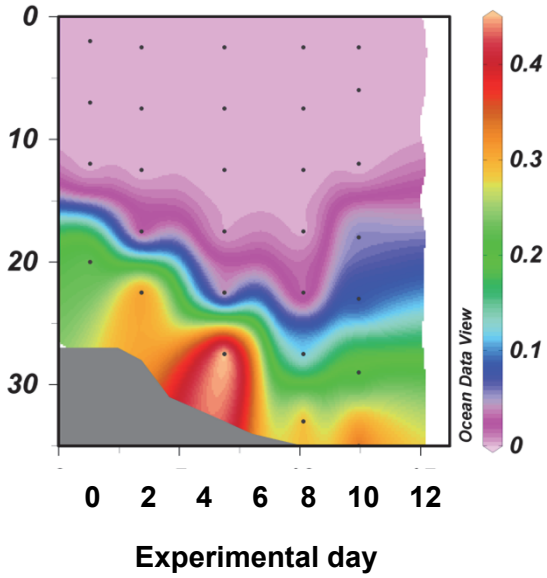

Bacterial abundance (x10^4 cells ml^{-1})

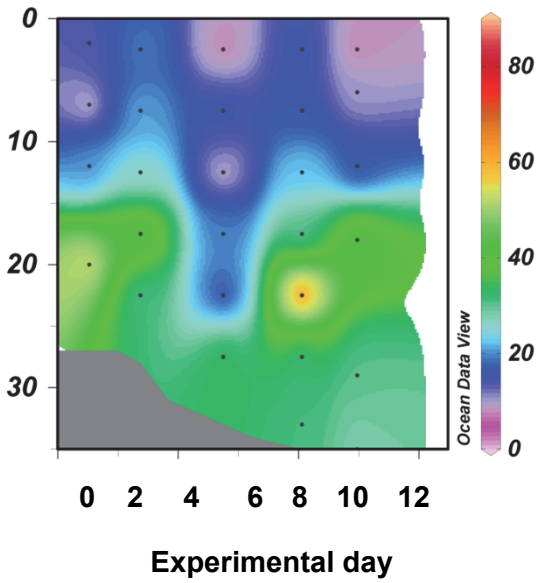

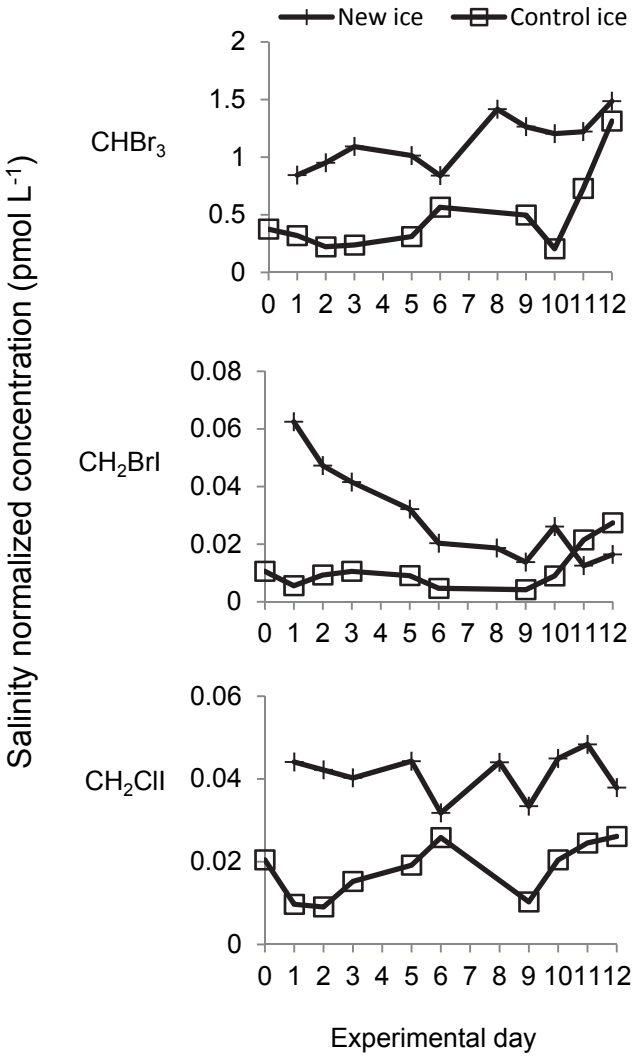
New ice
Control ice
Salinity normalized concentration (pmol L-1)
CHBr3
CH2BrI
CH2ClI
Experimental day